analytical chemistry

ARTICLE

pubs.acs.org/ac

Ultrafast Surface Enhanced Resonance Raman Scattering Detection in Droplet-Based Microfluidic Systems

Michael P. Cecchini,[†] Jongin Hong,[‡] Chaesung Lim,[§] Jaebum Choo,[§] Tim Albrecht,[∥] Andrew J. deMello,[∥] and Joshua B. Edel*[,∥]

[†]Materials Department and [∥]Department of Chemistry, Imperial College London, South Kensington Campus, London SW7 2AZ, United Kingdom

[‡]Department of Chemistry, Chung-Ang University, Seoul 156-756, Korea

[§]Department of Bionano Engineering, Hanyang University, Sa-1-dong, Ansan 426-791, Korea

Supporting Information

ABSTRACT: The development of ultrafast Raman-based detection is one of the most interesting challenges underpinning the application of droplet-based microfluidics. Herein, we describe the use of surface-enhanced resonance Raman spectroscopy (SERRS) with submillisecond time resolution as a powerful detection tool in microdroplet reactors. Individual droplets containing silver nanoparticle aggregates functionalized with Raman reporters are interrogated and characterized by full spectra acquisitions with high spatial resolution in real time. Whereas previous works coupling SERRS with droplet-based microfluidics acquire a single spectrum over single or multiple droplets, we build upon these results by increasing our temporal resolution by 2 orders of magnitude. This allows us to interrogate multiple points within one individual droplet. The SERRS signals emitted from the aggregates are utilized to access the influence of flow rate on droplet size and throughput. Accordingly, our approach allows for high-throughput analysis that facilitates the study of other biological assays or molecular interactions.

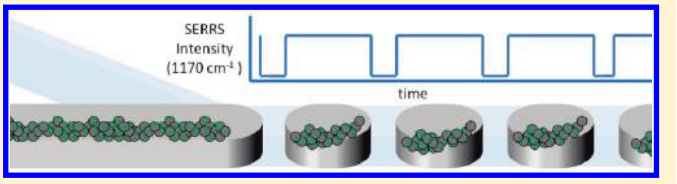

In the last 2 decades a range of microfabricated systems have been developed to perform ultrafast measurements on small sample volumes.[1−6] Compared to macroscale instrumentation, miniaturization of such systems creates significant advantages in terms of speed, throughput, yield, selectivity, and control. Notably, all these benefits are directly facilitated by improved heat and mass transfer associated with system downscaling. Recently, the manipulation of multiphase (or segmented) flow within microfluidic channels has attracted much attention, and indeed, such systems have been used to define new platforms for high-throughput experimentation.[7−12] In simple terms, segmented flow technology involves the compartmentalization of reagents of interest within submicroliter-sized droplets that reside within a continuous and immiscible fluid. Each droplet can be thought of as a test tube with a volume that can range from a few femtoliters to many nanoliters. Importantly, individual droplets can be produced at kilohertz frequencies and can be manipulated in a controlled manner by functional operations, such as droplet fission, fusion, sorting, and storage.[13−18] Although the development of droplet-based microfluidic systems is still in its infancy, the technology has been exploited in a diverse range of applications, including experimental biology[15−27] and nanomaterial synthesis.[28−30] In theory, droplet-based microfluidic technologies allow complex analytical procedures to be performed on ultrasmall sample volumes in an automated, reproducible, and rapid manner.[31] However, due to the high droplet generation rates that can be routinely accessed, the demands on detection protocols are significant. Indeed, the ability to probe each and every droplet in real time and with sufficient sensitivity is essential to extract and utilize the huge amounts of information produced from droplet-based microfluidic systems.[2] Accordingly, the exploitation of such platforms in high-throughput experimentation is normally limited by the available detection method. To date, a number of studies have reported the use of a variety of detection techniques for characterizing individual or multiple droplets. These include time-integrated and time-resolved fluorescence spectroscopy, Raman spectroscopy, and electrochemical detection.[15−24,31−42] The use of optical methods is well-suited for monitoring segmented flow, where droplets move with high linear velocities. Indeed, a fluorescence microscope equipped with a sensitive CCD camera is most commonly used for image capture in droplet-based experiments. Unfortunately, conventional CCD cameras are not fast enough to sensitively interrogate each droplet at high droplet generation rates. Moreover, high-speed cameras are expensive and lack sensitivity when compared to more conventional photomultiplier tubes (PMTs) and avalanche photodiode detectors (APDs). Recently, confocal fluorescence spectroscopy has been demonstrated to be able to accurately and precisely quantify droplets and their contents in a high-throughput

Received: December 23, 2010
Accepted: February 26, 2011
Published: March 17, 2011

fashion.[19−24,33−36] Additionally, Förster resonance energy transfer (FRET) has been used to analyze biological assays and enzyme kinetics,[20−23] and fluorescence lifetime imaging (FLIM) methods have been developed to analyze mixing patterns within droplets.[33,34] More recently, the reduction of laser-illuminated probe volumes has been used to permit the counting of single molecules in individual picoliter-sized droplets.[35,36] Unfortunately, all of the above rely on the presence of extrinsic or intrinsic fluorophores to report on analyte concentration or environment. Such a situation becomes problematic when performing multiplexed assays since multiple excitation sources and detectors are required. Additionally, fluorescence emission spectra are typically broad in the condensed phase and lack the ability to provide detailed structural information. In the light of these constraints, Raman spectroscopy offers several advantageous features for use in droplet-based microfluidics. On the basis of the inelastic scattering of light, Raman spectroscopy allows for the generation of highly resolved spectral fingerprints unique to the analyte under investigation. This creates the opportunity to distinguish between multiple analytes in complex samples with reduced instrumentation requirements (i.e., a single excitation source and a single detector are sufficient for multiplexed analysis). The extremely small cross sections associated with the Raman scattering process limit its use as an ultrasensitive detection technique under normal conditions. However, the more recent development of surface-enhanced Raman spectroscopy (SERS) has cross sections approximately 8 orders of magnitude greater than ordinary Raman scattering. Primarily caused by the augmentation of the electric field incident on the molecule generated by the excitation of localized surface plasmons in the metallic nanostructure geometry, the SERS intensities can be comparable with that of fluorescence. This sensitivity can further be increased by choosing the excitation frequency to match that of the electronic transition of the analyte, creating further resonance enhancement, referred to as surface-enhanced resonance Raman spectroscopy (SERRS). Nonetheless, its application in quantitative analysis is hampered by irreproducibility in signal enhancement due to a lack of control over factors such as the inhomogeneous distribution of molecules on metallic surfaces and the occurrence of nanoparticle aggregation (which results in inconsistent enhancements across the probed surface).

The integration of SERS detection with microfluidic analysis systems has recently been employed to alleviate adhesion of colloid/analyte conjugates on wall surfaces.[37−40] For example, Wang et al. have shown that such a system yields reproducible and quantitative results in terms of the detection of mercury(II) ions in water.[6,37] Strehle et al. have shown highly reproducible SERS experiments in a liquid/liquid segmented flow system using crystal violet as a model compound.[39] However, in order to reduce limits of detection, such Raman and SERS measurements are typically recorded using extended acquisition times greater than or equal to 1 second. This limits application in droplet-based microfluidics, where distinct droplets are generated at kilohertz frequencies and move with high linear velocities. Accordingly, the development of ultrafast Raman-based detection is one of the most interesting challenges associated with droplet-based microfluidics. To this end, we report the use of surface-enhanced resonance Raman spectroscopy (with submillisecond time resolution) as a powerful detection tool in droplet-based microfluidics.

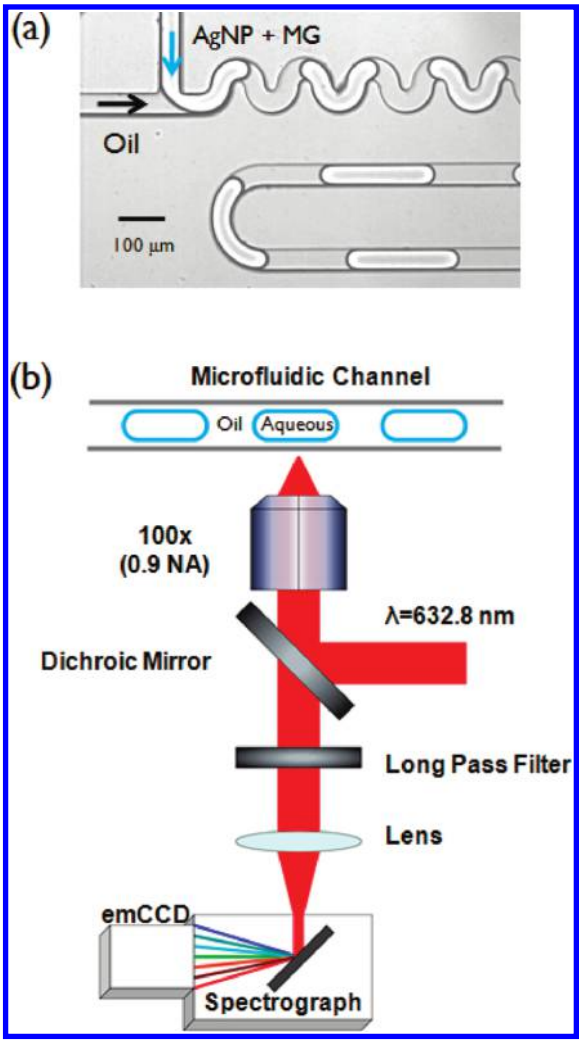

Figure 1. (a) An image of droplet generation within the microfluidic device and (b) a schematic of a home-built Raman spectrometer used for droplet interrogation.

EXPERIMENTAL SECTION

Microfluidic devices were prepared by polydimethylsiloxane (PDMS) molding from SU-8 masters. Access holes were punched into the PDMS channel ends with syringe needles. The PDMS slab was then bonded to a 160-μm microscope coverslip to allow efficient optical interrogation. The device layout consists of two inlets, a 50-μm-wide and 50-μm-deep channel and an outlet (Figure 1a). We use a T-junction geometry to generate aqueous droplets in a carrier fluid, a 10:1 (v/v) mixture of 3 M fluorinated FC-3283/EGC-1700 and 1*H*,1*H*,2*H*,2*H*-perfluorooctanol (PFO) for droplet experiments. To create the SERS substrates, silver nanoparticles were synthesized by reducing silver nitrate using hydroxoylamine hydrochloride at room temperature.[43] The average size of the produced silver nanoparticles was 35 ± 5 nm, as measured by transmission electron microscopy (see Figure S1 in the Supporting Information). To increase the number of hot spots contained on the silver nanoparticles, NaCl was used to decrease the electrostatic repulsion between nanoparticles promoting aggregation. Moreover, Malachite Green (MG) was used as the Raman reporter due to the additional resonance enhancement created by the dyes' strong optical absorption near the

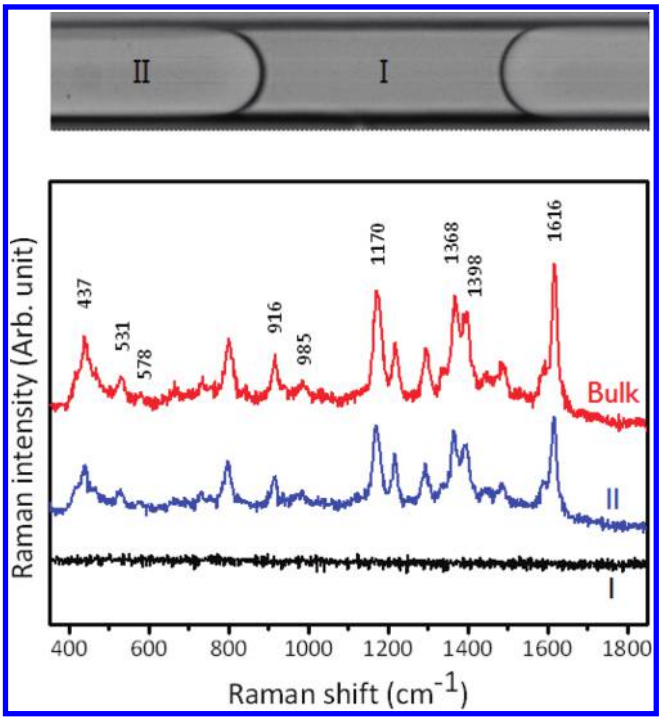

Figure 2. (Top) An example image of droplets generated using the microfluidic system. The channel width is 50 μm. (Bottom) Raman spectra of the continuous oil phase (I), 75 ppb MG in Ag nanocolloids within a segmented flow (II), and 75 ppb MG in Ag nanocolloids in bulk solution (Bulk). An exposure time of 10 μs was used in all cases.

excitation frequency. A mixture of silver colloids, NaCl, and MG was injected through the aqueous inlet using a precision syringe pump (PHD 2000, Harvard Apparatus). Volumetric flow rates of oil and aqueous channels were varied from 4 to 10 μL/min to control both droplet size and frequency.

SERRS measurements were performed using a home-built Raman microscope consisting of an inverted microscope (IX71, Olympus) equipped with a 100× air objective with a numerical aperture of 0.9 (MPLFLN100×, Olympus). The monochromatic light source used in all experiments was a HeNe laser (HRP170, Thorlabs), which emitted linearly polarized light at 632.8 nm. The laser power measured at the sample was 8.5 mW. Entrance optics consists of two bandpass filters (LL01-633-12.5, Semrock) to prevent stray light from entering the system and a dichroic mirror (LDP01-633RU-25 × 36 × 2.0, Semrock) to redirect the excitation path into the microscope objective. The Raman scattered light is collected through the same objective and sent through a long-pass filter (LP02-633RU-25, Semrock) to remove the anti-Stokes and Rayleigh scattered light. Finally, a lens focuses the scattered light into the entrance slit of a Czerny−Turner spectrograph (Shamrock-303i, Andor), which routes radiation onto an Electron Multiplying CCD (Newton DU970N-BV, Andor). A custom algorithm developed in MatLab (Mathwork, Cambridge, UK) was used to correct for background in each individual acquisition frame. This algorithm is also used to identify peaks of interest and discriminate between background and droplet signatures. This allows extraction of droplet-generation frequencies, time-differences between droplets, and size distributions.

RESULTS AND DISCUSSION

MG is a C_2 symmetric triphenylmethane (TPM) dye that exhibits fast nonradiative relaxation after photoexcitation.[44,45] In the current study, the clustering and aggregation of nanoparticles take place in an aqueous solution upon addition of MG. Subsequently, this mixture was injected into the microfluidic device to verify ultrarapid SERRS detection of individual droplets. Figure 2 shows SERRS spectra of 75 ppb MG adsorbed onto silver nanoparticles between 350 and 1850 cm^{-1} (without background subtraction). The prominent band at 1616 cm^{-1} originates from in-plane C−C (in-phase) stretching vibrations located within the three phenyl rings.[46] The normal coordinate is symmetric, and thus, the associated Raman cross-section is high. Peaks at 1170 and 1368 cm^{-1} are associated with in-plane ring C−H bending and N−phenyl stretching vibrations, respectively.[46] The peak at 1398 cm^{-1} originates due to an overlap of the in-plane phenyl C−C and N−phenyl stretching vibrations, and the peak at 437 cm^{-1} is due to Ph−C^+−Ph out-of-plane bending vibrations.[46] Smaller intensity peaks observed at 531, 578, 916, and 985 cm^{-1} are assigned to the ring skeletal vibrations of radical orientations.[46] It should be noted that these molecular fingerprints are highly valuable in identifying the interrogated molecules in a label-free manner.

Table 1. Refractive Indices of Fluids and Materials Used in This Study

oil phase[a]	Ag NP soln	MG	Ag NP soln + MG	PDMS
1.281	1.331	1.332	1.3315	1.47

[a] A mixture of FC3283/EGC-1700 and PFO.

Spectrum I in Figure 2 was measured from the oil phase and exhibits no significant peaks, while spectrum II was obtained from the aqueous droplets containing 75 ppb MG. Droplets were generated at a volumetric flow rate of 1.5 μL/min (for both the aqueous and oil phases). The total volumetric flow rate was kept at 3 μL/min and the water fraction was 0.5. The water fraction (W_f) is defined as $W_f = F_w/(F_w + F_o)$, where F_w and F_o are the aqueous- and oil-phase flow rates, respectively. It should be noted that the PDMS substrate will also exhibit a Raman spectrum, and thus, the excitation beam was tightly focused within the microchannel using the high NA 100× objective. Any signal from the PDMS substrate can be effectively removed though implementation of a confocal pinhole. However, this was not necessary in the current experiments, since the channel depth was significantly greater than the depth of focus of the objective. We observed that the Raman peak intensities originating from droplets were 78 ± 3.5% of those from bulk samples using the same acquisition parameters. This reduction can be attributed to interference from surrounding fluids. Additionally, refraction of light passing through liquid−solid or liquid−liquid interfaces or both will cause the reduction of Raman intensity from the droplet. The refractive indices of all materials used in this study are provided in Table 1. The oil phase used in this study has the lowest refractive index, and thus, if we adopt an oil phase having the same refractive index as the aqueous phase (called refractive index matching oil) in SERS-based droplet experiments, refraction issues can be minimized. However, refractive index varies with temperature and wavelength of light and the change in the oil phase also influences current droplet generation conditions. Currently, we are exploring the scheme of refractive index matching for droplet-based microfluidics.

To determine the influence of flow rate on microdroplet throughput, average pulse widths and detection events per unit time were analyzed. Figure 3 shows time traces of a sequence of droplets containing 75 ppb MG for three different volumetric flow rates over a 2 s window. The total volumetric flow rate of the aqueous and oil phases was varied to change both the droplet generation frequency

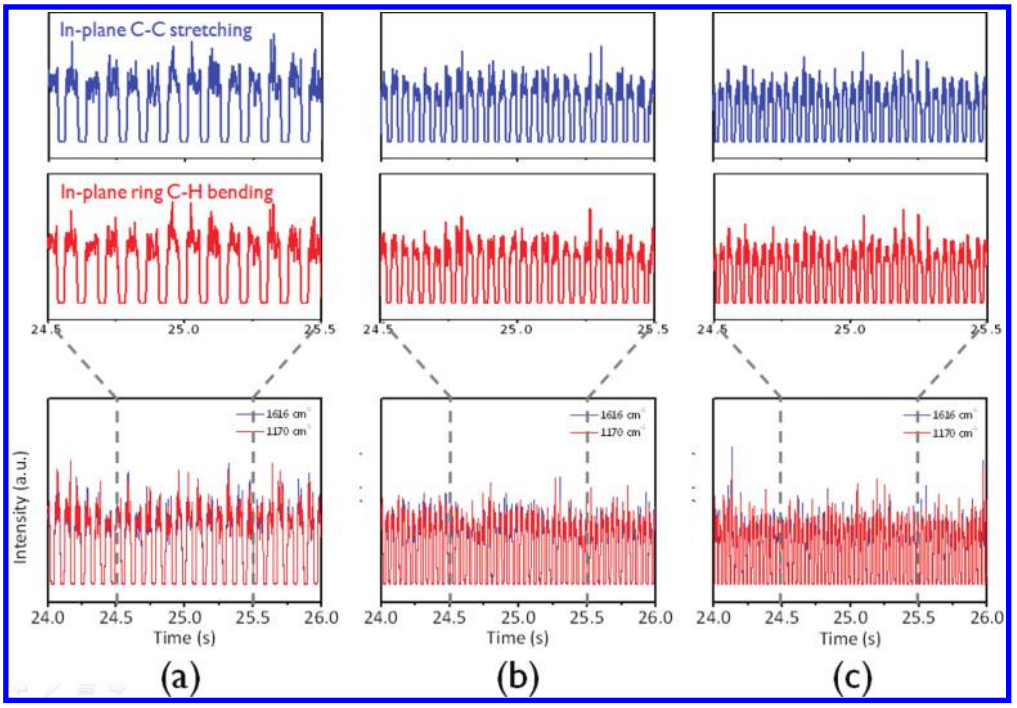

Figure 3. Time traces of SERRS signals from 75 ppb MG over a time period of 2 s for total flow rates of (a) 4 μL/min, (b) 6 μL/min, and (c) 8 μL/min. Each inset illustrates an expanded 1 s part of the main trace. Blue and red signals correspond to in-plane C−C stretching and C−H bending vibrations, respectively.

and droplet size, while the water fraction (W_f) was kept constant at 0.5. Good discrimination between the aqueous droplets and the continuous oil phase is observed for all fluidic conditions. As expected, the average pulse width corresponding to a single microdroplet decreases with increasing flow rate. For the same acquisition duration of 47.5 s, 632 microdroplets were detected using a 4 μL/min flow rate and 1194 and 1557 microdroplets for the 6 and 8 μL/min, respectively. Pulse widths under the total flow rate of 4, 6, and 8 μL/min were 49.1 $\pm$ 1.7, 25.8 $\pm$ 0.62, and 20.4 $\pm$ 1.2 ms, respectively (see Figure S2 in the Supporting Information). This indicates uniform droplet generation frequency and monodisperse droplet size distribution. Importantly, the ability to acquire full Raman spectra multiple times from a single droplet has never been achieved elsewhere when compared to previous droplet experiments with SERS detection.[37−40] Notably, the recorded SERRS signal is highly uniform within individual droplet and reproducible between experiments. The uniformity of the droplet signature is highlighted in the expanded segments shown in the insets of Figure 3. Blue (top) and red (bottom) signals correspond to vibrations at 1170 cm^{-1} (in-plane ring C−H bending) and 1616 cm^{-1} (in-plane C−C stretching), respectively. This suggests significant potential for use in multiplexed analyses or in reactions where the vibration frequency changes using a single excitation source. Average signal intensities for identical exposure times were also observed to be independent of total flow rate. For example, average SERRS intensities for the 1616 cm^{-1} peak are 2053, 1898, and 1807 counts with standard deviations of 54, 50, and 48 counts for 4, 6, and 8 μL/min, respectively. It should be noted that droplet generation frequencies and SERRS pulse widths measured by SERRS detection as discussed above were comparable with those determined using a high-speed camera.

While previous works represent an ensemble of whole Raman spectra that is blind to the occurrence of subpopulations in SERS events, we performed multiple acquisitions within a single droplet with submilisecond time resolution. Our rapid detection enabled us to collect 52, 27, and 21 full spectrum frames for one individual droplet under the total flow rate of 4, 6, and 8 μL/min, respectively. The substantial amounts of SERRS data collected from the single droplet were used to study the aggregation behavior of the nanoparticles at a high spatial resolution. As the SERRS intensity is dependent on the aggregation arrangement, quality control of the aggregation process is therefore critical to ensure reliable and repeatable SERS responses. Recently, Goddard et al. showed the correlation between SERRS intensities and background fluctuations by taking full spectra acquisitions of nanoparticles in flow.[47] They verified that the background fluctuations in relation to peak intensity fluctuations are attributed to different nanoparticle aggregate geometries.

In order to characterize the nanoparticle aggregates inside the microdroplets, we evaluated how peak intensities correlated with background fluctuations and how intensity changes at one peak correlated with those at other peaks. Within just a single droplet, a strong correlation between SERRS intensity and background fluctuations was noticed when comparing the intensity of the 1616 cm^{-1} peak to that of the nearby background region at 1719 cm^{-1}. This suggests that much of the fluctuations in the SERRS intensity result from different nanoparticle aggregate geometries within the droplet. This analysis was carried out, and the correlated Raman intensities of all interrogated droplets under the flow rate of 4 μL/min are shown in Figure 4a. Additional background points also show the same correlation. This analysis shows the strength of using microdroplets to analyze the SERRS geometries. Although each droplet contained the same nanoparticle aliquot in our case, loading the droplets with different samples would create a high-throughput platform to investigate the effect of different aggregation promoters and labeling concentrations on the nanoparticle geometries. The repeatability in our results also represents the accuracy of such platform. Moreover, to show the

dx.doi.org/10.1021/ac103329b |*Anal. Chem.* 2011, 83, 3076–3081

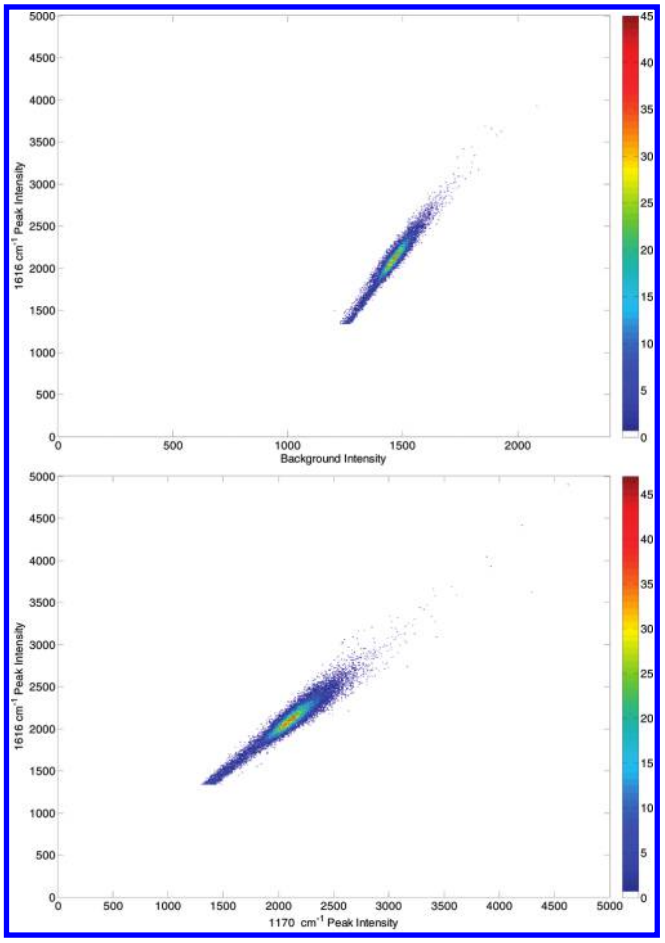

Figure 4. (a) SERRS intensities of the 1616 cm^{-1} vibrational band plotted against the 1719 cm^{-1} background intensity under that total flow rate of 4 μL/min. A strong correlation between background intensity and peak intensity indicates the presence of different nanoparticle aggregate geometries within the microdroplets. (b) Intensities of the 1616 cm^{-1} peak vs the 1170 cm^{-1} peak under the total flow rate of 4 μL/min. A strong correlation between peak intensities indicates an equal enhancement provided by the nanoparticle aggregate on the dye. Using this methodology within a droplet creates a controllable, high-throughput platform for Raman dye investigation.

potential for multiplexed analysis using a single excitation source with microdroplets, the spectral variability of the 1170 cm^{-1} and 1616 cm^{-1} vibrational modes of MG was also analyzed. Figure 4b illustrates a strong correlation in peak intensity of the two vibrational modes when total flow rate is 4 μL/min (i.e., the strong correlation was also verified in the cases of 6 and 8 μL/min). This suggests a stable spectral response of MG among aggregates and an equal enhancement of both vibrational bands. Additionally, this analysis can be applied to other vibrational modes from the full spectra acquisition. The strong intensity correlation between the 1170 and 1616 cm^{-1} vibrational bands also holds true for the other vibrational bands of MG (not shown), revealing the benefits of acquiring full spectra acquisitions. Additionally, variability between different dyes can also be studied by varying the dye loaded into microdroplets.

Herein, our focus was to verify the efficient analysis of individual picoliter-volume droplets in continuous flow using SERRS. The time resolution for the current experiments is limited by the CCD detector. We are able to successfully achieve submillisecond, full-spectrum Raman analysis by cropping and binning the CCD sensor to reduce the number of pixels required for readout. While spectral resolution reduces as a function of pixel binning, spectral resolution is maintained by limiting the number of binned pixels. To account for the decreased acquisition times demanded by rapid frame rates, electron multiplying gain was used to decrease readout noise. In addition, statistical analysis of the time traces can be performed in a direct manner. For example, probability histograms of pulse width as a function of the oil flow rate demonstrate excellent monodispersity in SERRS pulse widths (Figure 3 and Supporting Information, Figure S2). This width correlates with droplet size (assuming that the average droplet velocity is constant) or droplet speed (assuming that the droplet size is constant). Using full-spectra acquisitions with a high-throughput platform also allows statistical analysis to be performed on the acquired data from individual droplets.

CONCLUSION

In conclusion, we have demonstrated a novel, high-throughput, droplet-based SERRS detection platform. The approach allows for online characterization and detection of droplets with submillisecond time resolution. Individual droplets generated within a segmented flow can be monitored and characterized (in terms of their vibrational fingerprint) in real time. This general approach to high-throughput, label-free droplet analysis is expected to be readily extended to the study of other biological assays or molecular interactions. Since small-volume droplets of varying composition can be generated in a rapid fashion, studies of biological interactions within droplets at low analytical concentrations are an appealing possibility and pave the way for a new generation of droplet-based microfluidic system.

In practice, droplet-based microfluidic systems facilitate uniform and controlled mixing of reagents within the microfluidic network. When performing synthetic processes in current droplet-based formats, reagents are injected together in a confluent stream just prior to droplet generation with the reaction occurring at later times. Interestingly, when such designs are used, contact between the nanocolloid and analyte streams before droplet generation causes the aggregation of nanoparticles at the interface due to diffusive mixing (see Figure S3 in the Supporting Information). Thus, we expect that this can be resolved by pairing of individual droplets, such as nanocolloids and analytes, and subsequent fusion/mixing in a microfluidic network.[48] Moreover, we are also currently exploiting our approach in multiplexed detection, with these studies forming the basis of a future publication.

ASSOCIATED CONTENT

Supporting Information. Figures S1−S3, as discussed in the text. This material is available free of charge via the Internet at http://pubs.acs.org.

AUTHOR INFORMATION

Corresponding Author

*E-mail: joshua.edel@imperial.ac.uk.

ACKNOWLEDGMENT

M.P.C. and J.H. contributed equally to this work. This work was supported by the RCUK Microdroplets Basic Technology Project. The authors also acknowledge the National Research Foundation of Korea (Grant Numbers R11-2009-044-1002-0K20904000004-09A050000410). J.H. acknowledges the Brain

Korea 21 Project. The authors acknowledge Prof. David McComb for his useful discussion. M.P.C. and J.H. contributed equally toward this publication.

REFERENCES

(1) Whitesides, G. M. *Nature* **2006**, *442*, 368–373.
(2) deMello, A. J. *Nature* **2006**, *442*, 394–402.
(3) Hong, J.; Edel, J. B.; deMello, A. J. *Drug Discovery Today* **2009**, *14*, 134–146.
(4) Arora, A.; Simone, G.; Salieb-Beugelaar, G. B.; Kim, J. T.; Manz, A. *Anal. Chem.* **2010**, *82*, 4830–4847.
(5) Salieb-Beugelaar, G. B.; Simone, G.; Arora, A.; Philippi, A.; Manz, A. *Anal. Chem.* **2010**, *82*, 4848–4864.
(6) Lim, C.; Hong, J.; Chung, B. G.; deMello, A. J.; Choo, J. *Analyst* **2010**, *135*, 837–844.
(7) Song, H.; Chen, D. L.; Ismagilov, R. F. *Angew. Chem., Int. Ed.* **2006**, *45*, 7336–7356.
(8) Gunther, A.; Jensen, K. F. *Lab Chip* **2006**, *6*, 1487–1503.
(9) Huebner, A.; Sharma, S.; Srisa-Art, M.; Hollfelder, F.; Edel, J. B.; deMello, A. J. *Lab Chip* **2008**, *8*, 1244–1254.
(10) Shaerli, Y.; Hollfelder, F. *Mol. Biosyst.* **2009**, *5*, 1392–1404.
(11) Chiu, D. T.; Lorenz, R. M. *Acc. Chem. Res.* **2010**, *42*, 649–658.
(12) Theberge, A. B.; Courtois, F.; Schaerli, Y.; Fischlechner, M.; Abell, C.; Hollfelder, F.; Huck, W. T. S. *Angew. Chem., Int. Ed.* **2010**, *49*, 2–25.
(13) Link, D. R.; Anna, S. L.; Weitz, D. A.; Stone, H. A. *Phys. Rev. Lett.* **2004**, *92*, 054503–4.
(14) Fidalgo, L. M.; Whyte, G.; Brantton, D.; Kaminski, C. F.; Abell, C.; Huck, W. T. S. *Angew. Chem., Int. Ed.* **2008**, *48*, 3665–3668.
(15) Niu, X. Z.; Gielen, F.; deMello, A. J.; Edel, J. B. *Anal. Chem.* **2009**, *81*, 7321–7325.
(16) Huebner, A.; Bratton, D.; Whyte, G.; Yang, M.; deMello, A.J.; Abell, C.; Hollfelder, F. *Lab Chip* **2009**, *9*, 692–698.
(17) Baret, J. C.; Miller, O. J.; Taly, V.; Ryckelynck, M.; El-Harrk, A.; Frenz, L.; Rick, C.; Samuels, M. L.; Hutchison, B.; Agresti, J. J.; Link, D. R.; Weitz, D. A.; Griffiths, A. D. *Lab Chip* **9, 2009**, 1850–1858.
(18) Bai, Y. P.; He, X. M.; Liu, D. S.; Patil, S. N.; Bratton, D.; Huebner, A.; Hollfelder, F.; Abell, C.; Huck, W. T. S. *Lab Chip* **2010**, *10*, 1281–1285.
(19) Huebner, A.; Srisa-Art, M.; Holt, D.; Abell, C.; Hollfelder, F.; deMello, A. J.; Edel, J. B. *Chem. Commun.* **2007**, 1218–1220.
(20) Srisa-Art, M.; deMello, A. J.; Edel, J. B. *Anal. Chem.* **2007**, *79*, 6682–6689.
(21) Srisa-Art, M.; Dyson, E. C.; deMello, A. J.; Edel, J. B. *Anal. Chem.* **2008**, *80*, 7063–7067.
(22) Hsieh, A. T.-H.; Pan, P.J.-H.; Lee, A. P. *Microfluid. Nanofluid.* **2009**, *6*, 391–401.
(23) Srisa-Art, M.; Kang, D. K.; Hong, J.; Park, H.; Leatherbarrow, R. J.; Edel, J. B.; Chang, S.-I.; deMello, A. J. *ChemBioChem* **2009**, *10*, 1605–1611.
(24) Srisa-Art, M.; Bonzani, I. C.; Willams, A.; Stevens, M. M.; deMello, A. J.; Edel, J. B. *Analyst* **2009**, *134*, 2239–2245.
(25) Hong, J.; deMello, A.J.; Jayasinghe, S.N.; , *Biomed. Mater.*, **2010**, *5*, 021001(1−6).
(26) Agresti, J. J.; Antipov, E.; Abate, A. R.; Ahn, K.; Rowat, A. C.; Baret, J. C.; Marquez, M.; Klibanov, A. M.; Griffith, A. D.; Weitz, D. A. *Proc. Natl. Acad. Sci. U. S. A.* **2010**, *107*, 4004–4009.
(27) Chan, E. M.; Alivvisatos, A. P.; Mathies, R. A. *J. Am. Chem. Soc.* **2005**, *127*, 13854–13861.
(28) Hung, L.-H.; Choi, K. M.; Tseng, W.-Y.; Tan, Y.-C.; Shea, K. J.; Lee, A. P. *Lab Chip* **2006**, *6*, 174–178.
(29) Frenz, L.; Harrak, A. E.; Pauly, M.; Begin-Colin, S.; Griffiths, A. D.; Baret, J.-C. *Angew. Chem., Int. Ed.* **2008**, *47*, 6817–6820.
(30) Dove, A. *Nat. Biotechnol.* **1999**, *17*, 859–863.
(31) Song, H.; Ismagilov, R. F. *J. Am. Chem. Soc.* **2003**, *125*, 14613–14619.
(32) Liau, A.; Karnik, R.; Majumdar, A.; Cate, J. H. D. *Anal. Chem.* **2005**, *77*, 7618–7625.
(33) Srisa-Art, M.; deMello, A. J.; Edel, J. B. *Phys. Rev. Lett.* **2008**, *101*, 014502.
(34) Solvas, X. C.; Srisa-Art, M.; deMello, A. J.; Edel, J. B. *Anal. Chem.* **2010**, *82*, 3950–3956.
(35) Srisa-Art, M.; deMello, A. J.; Edel, J. B. *Chem. Commun.* **2009**, 6548–6550.
(36) Rane, T. D.; Puleo, C. M.; Liu, K. J.; Zhang, Y.; Lee, A. P.; Wang, T. H. *Lab Chip* **2010**, *10*, 161–164.
(37) Wang, G.; Lim, C.; Chen, L.; Chon, H.; Choo, J.; Hong, J.; deMello, A. J. *Anal. Bioanal. Chem.* **2009**, *394*, 1827–1832.
(38) Ackermann, K. R.; Henkel, T.; Popp, J. *ChemPhysChem* **2007**, *8*, 2665–2670.
(39) Strehle, K. R.; Cialla, D.; Rosch, P.; Henkel, T.; Kohler, M.; Popp, J. *Anal. Chem.* **2007**, *79*, 1542–1547.
(40) Marz, A.; Ackermann, K. R.; Malsch, D.; Bocklitz, T.; Henkel, T.; Popp, J. *J. Biophoton.* **2009**, *2*, 232–242.
(41) Luo, C. X.; Yang, X. J.; Fu, O.; Sun, M. H.; Ouyang, Q.; Chen, Y.; Ji, H. *Electrophoresis* **2006**, *27*, 1977–1983.
(42) Liu, S.; gu, Y.; Roux, R. B. L.; Mattews, S. M.; Brantton, D.; Yunus, K.; Fisher, A. C.; Huck, W. T. S. *Lab Chip* **2008**, *8*, 1937–1942.
(43) Lee, S.; Choi, J.; Chen, L.; Park, B.; Kyong, J. B.; Seong, G. H.; Choo, J.; Lee, Y.; Shin, K.-H.; Lee, E. K.; Joo, S.-W.; Lee, K.-H. *Anal. Chim. Acta* **2007**, *590*, 139–144.
(44) Nagasawa, Y.; Ando, Y.; kataoka, D.; Matsuda, H.; Miyasaka, H.; Okada, T. *J. Phys. Chem. A* **2002**, *106*, 2024–2035.
(45) Sen, P.; Yamaguchi, S.; Tahara, T. *Faraday Discuss.* **2010**, *145*, 411–428.
(46) Schneider, S.; Brehm, G.; Freunscht, P. *Phys. Status Solidi B* **1995**, *189*, 37–42.
(47) Goddard, G.; Brown, L. O.; Habbersett, R.; Brady, C. I.; Martin, J. C.; Graves, S. W.; Freyer, J. P.; Doorn, S. K. *J. Am. Chem. Soc.* **2010**, *132*, 6081–6090.
(48) Hong, J.; Choi, M.; Edel, J. B.; deMello, A. J. *Lab Chip* **2010**, *10*, 2702–2709.